Elastic Scattering of O^{16} from Nuclei*

J. A. McIntyre, S. D. Baker, and T. L. Watts
Yale University, New Haven, Connecticut
(Received July 1, 1959)

O^{16} nuclei have been elastically scattered from Au^{197}, Ni (natural isotope abundance), Al^{27}, and C^{12} at a laboratory energy of 158 Mev. The angular distributions obtained show features similar to those obtained for alpha particles scattered from various nuclei. However, diffraction effects are evident for target nuclei of higher atomic number Z with the alpha particle as the bombarding nucleus than with O^{16} as the bombarding nucleus. A survey of the literature is presented to show that diffraction effects become evident for $\eta \lesssim 5$, where $\eta \equiv ZZ'e^2/\hbar v$.

I. INTRODUCTION AND CONCLUSIONS

IN this paper experiments are reported of O^{16} nuclei elastically scattered from Au^{197}, Ni (natural abundance), Al^{27}, and C^{12}. The results obtained from these experiments have then been compared to previous scattering results from the literature where alpha particles and other heavier nuclei have been used as the bombarding particles.

The work on the elastic scattering of alpha particles and heavier nuclei has been reactivated recently by Farwell and Wegner.[1,2] They investigated high-Z nuclei by scattering alpha particles with energies up to 40 Mev. These experiments yielded the usual Rutherford scattering for classical trajectories outside a nuclear radius R, while for trajectories passing inside this radius, the scattering cross section rapidly dropped below the Rutherford value. Just before the drop away from the Rutherford scattering the scattering cross section also was found to rise 10–20% above the Rutherford value. These features were successfully described theoretically by Blair[3] by means of a partial wave analysis of the scattering, using a sharp cutoff at the "nuclear radius." All partial waves with classical trajectories passing inside this radius were assumed to be absorbed or eliminated by the nucleus. Further experiments at various energies yielded alpha-particle elastic scattering angular distributions for high-Z elements with similar features.[4–9] Although the theoretical sharp-cutoff model produced the features described above, it also yielded oscillations about a constant cross section after dropping about a factor of ten below the Rutherford value. This feature of the model was in contradiction, of course, to the continued drop-off of the experimental cross sections.

Scattering of alpha particles from elements of lower Z revealed a qualitatively different result.[10–14] For these elements marked diffraction structure appeared. These later experiments also covered intermediate-Z elements which showed small diffraction structure superimposed on a rapid drop away from Rutherford scattering, i.e., a combination of the high-Z and low-Z results. Further calculations with the sharp-cutoff model showed that the experimental diffraction structure for the low-Z elements coincided roughly with the diffraction oscillations of the sharp-cutoff model.[15] However, the experimental data did not extend to small enough angles to determine whether there was still a sharp drop-off below the Rutherford value.

Experiments have also been performed with heavier nuclei as the bombarding particle.[16,17] The high-Z behavior described for alpha-particle bombardment has been found to persist for both N^{14} scattered from N^{14} and for C^{12} scattered from Au^{197}.

Recently, calculations[18–21] have shown that the experimental features of the scattering can be reproduced rather well by using an optical model potential for the target nucleus. The relation between the optical model and sharp-cutoff model has also been pointed out.[15,19]

The experiments being reported here are for O^{16} nuclei scattered from both high-Z and low-Z nuclei. Only qualitative results will be considered at this time because of experimental uncertainties in normalizing the data. However, it can be shown clearly that the qualitative features obtained here fit in with the qualitative features of the scattering experiments just discussed. In addition, it will be shown that these features depend chiefly on one parameter,[22] $\eta \equiv ZZ'e^2/\hbar v$,

[1] G. W. Farwell and H. E. Wegner, Phys. Rev. 93, 356 (1954).
[2] G. W. Farwell and H. E. Wegner, Phys. Rev. 95, 1212 (1954).
[3] J. S. Blair, Phys. Rev. 95, 1218 (1954).
[4] Wall, Rees, and Ford, Phys. Rev. 97, 726 (1955).
[5] Wegner, Eisberg, and Igo, Phys. Rev. 99, 825 (1955).
[6] R. E. Ellis and L. Schecter, Phys. Rev. 99, 1044 (1955).
[7] R. E. Ellis and L. Schecter, Phys. Rev. 101, 636 (1956).
[8] H. E. Gove, Phys. Rev. 99, 1353 (1955).
[9] Kerlee, Blair, and Farwell, Phys. Rev. 107, 1343 (1957).

[10] E. Bleuler and D. J. Tendam, Phys. Rev. 99, 1605 (1955).
[11] Eisberg, Igo, and Wegner, Phys. Rev. 99, 1606 (1955).
[12] Igo, Wegner, and Eisberg, Phys. Rev. 101, 1508 (1956).
[13] Seidlitz, Bleuler, and Tendam, Phys. Rev. 110, 682 (1958).
[14] Gailar, Bleuler, and Tendam, Phys. Rev. 112, 1989 (1958).
[15] J. S. Blair, Phys. Rev. 108, 827 (1957).
[16] H. L. Reynolds and A. Zucker, Phys. Rev. 102, 1378 (1956).
[17] E. Goldberg and H. L. Reynolds, Phys. Rev. 112, 1981 (1958).
[18] G. Igo and R. M. Thaler, Phys. Rev. 106, 126 (1957).
[19] N. B. Cheston and A. E. Glassgold, Phys. Rev. 106, 1215 (1957).
[20] C. E. Porter, Phys. Rev. 112, 1722 (1958).
[21] G. Igo, Phys. Rev. Letters 1, 72 (1958).
[22] Igo, Wegner, and Eisberg, reference 12, have already shown that the magnitude of the diffraction structure depends on Z and v.

where Z and Z' are the atomic numbers of the target and bombarding nuclei, respectively, v is the relative velocity between these nuclei, and e and $\hbar$ have their usual meanings. Thus, a large η, or strong interaction, yields the sharp drop below Rutherford scattering; this situation approaches the classical picture of absorption of particles striking the nucleus. On the other hand, the small η or weak interaction case yields diffraction structure; this situation, in the limit, approaches the scattering of a plane wave from a black sphere with the attendant diffraction pattern.

II. EXPERIMENTAL APPARATUS

A. General Description

A schematic diagram of the experimental apparatus is shown in Fig. 1. The beam of oxygen ions from the heavy-ion accelerator at the left strikes a stripping foil after leaving the accelerator. (The stripping foil is 0.00025-in. aluminum-coated Melinex.[23]) The foil strips the last few electrons from the ions that are leaving the accelerator so that almost all of the ions have eight charges. These bare O^{16} nuclei are then deflected by the deflecting magnet through an angle of 31° and focussed horizontally and vertically at the slit position.[24] The magnet disperses horizontally the O^{16}'s of different energy such that a 0.25-in. wide slit will pass a 1% spread in energy. The beam energy was determined to be 158±2 Mev.[25]

After passing through the slits, the O^{16} beam strikes the target and is scattered. The target holder can be moved vertically so as to place any one of three different targets in the beam without breaking the vacuum of the scattering chamber. The target is always set with its plane perpendicular to the beam.
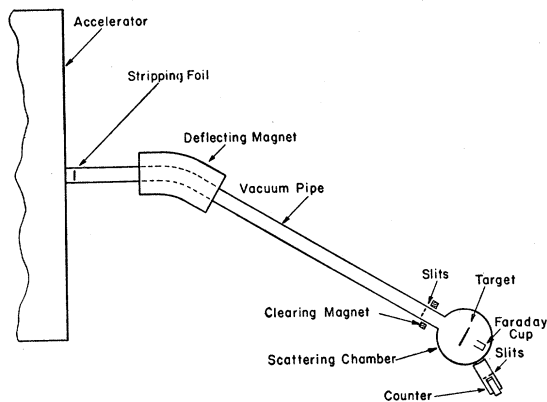

FIG. 1. Schematic diagram of the experimental apparatus.

---

[23] Obtained from Alexander Vacuum Research, Inc., New York, New York.

[24] The beam is focussed both horizontally and vertically at the slits if a parallel beam enters the deflecting magnet. The raw accelerator beam is found to focus into a $\frac{1}{4}$-in. diameter spot at the slits. Introduction of the stripping foil should increase the spot size about 10% due to multiple scattering in the foil.

[25] Anderson, Knox, and Quinton (private communication).

Beyond the target the beam strikes a Faraday cup. Four Faraday cups, ranging in diameter from $1\frac{1}{2}$ in. to $\frac{1}{2}$ in., are mounted on a vertical rod so that cups of various size can be inserted into the beam. The small cups are required when scattering at small angles is to be investigated. Thus far, the Faraday cups have not been checked for beam collection efficiency. Also, undoubtedly many electrons knocked out of the target are collected in the cup, thereby giving an incorrect beam intensity reading. The reading from the Faraday cup has thus far usually been used to give the accelerator operator a signal. The monitoring of the beam for the scattering experiment itself is done by collecting the charge from the target (which is insulated) on a polystyrene-insulated capacitor and measuring the capacitor voltage with a vibrating reed electrometer.[26] Presumably, the charge from the target is a measure of the number of electrons knocked out of the target by the beam and hence a measure of the beam itself. Electrons, that may be in the beam already because of the beam striking the slits, are removed by a clearing magnet prior to the target (see Fig. 1) so that no electrons will strike the target and falsify the monitor reading of the beam.

The scattering chamber is 8 in. in diameter with the target at the center. A 1-in. high by 0.001-in. thick Mylar ($C_{10}H_6O_4$) window extends around the chamber from 10° on the left of the beam direction to 150° on the right of the beam direction.

The scattered O^{16}'s are detected by a CsI(Tl) scintillation counter placed outside of the scattering chamber (see Fig. 1) at a distance of 21.1 in. from the center of the target. An evacuated pipe extends from the counter to the scattering chamber. A 0.001-in. Mylar window with $\frac{1}{2}$-in. diameter aperture allows scattered O^{16}'s leaving the scattering chamber to enter the counter pipe and strike the scintillator. A piece of 0.00025-in. aluminum-coated Melinex also covers the window to keep light away from the scintillator. The air gap between the scattering chamber and the counter pipe is 0.75 in. The CsI(Tl) scintillator is 0.010 in. thick by $1\frac{1}{2}$ in. in diameter and is glued to a $\frac{1}{4}$-in. thick Lucite disk of the same diameter.[27] Dow-Corning silicone oil is used as an optical coupling between the Lucite disk and an RCA-6342 photomultiplier. A $\frac{1}{4}$-in. diameter aperture mounted on the face of the CsI(Tl) scintillator limits the sensitive area of the detector to this region. The counter is surrounded by $\frac{1}{4}$ in. of steel for magnetic shielding. Pulses from the detector are fed through a cathode follower and a coaxial cable to the experimental control area and analyzed with a Baird-Atomic Model-520 20-channel analyzer. This fast analyzer (dead time

---

[26] Cary Electrometer, Model 31, Applied Physics Corporation, Pasadena, California.

[27] Obtained from Harshaw Chemical Company, Cleveland, Ohio.

TABLE I. Energy spread in the scattering process.

1 Target element	2 Target thickness (mg/cm²)	3 Target ΔE (Mev)	4 Beam ΔE (Mev)	5 Total[a] ΔE (Mev)
Au¹⁹⁷	2.29	2.6	1.6	2.6
Ni	2.23	4.0	1.6	4.0
Al²⁷	1.21	2.7	1.6	2.7
C¹² (CH₂)	1.01	2.7	1.6	2.7

[a] Full width at half maximum.

30 μsec in each channel) is used to facilitate rapid collection of data.

The detector is mounted on a heavy table which can be rotated about the target by remote control. The table swings around a bearing mounted in the fixed center post of the apparatus which supports the scattering chamber. The table is supported by two wheels as well as the bearing. The wheels roll on a 40-in. diameter track. The table will carry 1500 lb. of shielding. It was found, however, that no shielding is required. The angular position of the counter can be read remotely. A gear rack with 1400 teeth is wrapped around the track supporting the table. A pinion engaged in the rack is mounted to the table; the rotation of the pinion thus indicates the angular rotation of the counter about the target. A Selsyn, coupled to the pinion shaft, transmits the rotation to the experimental control area and the rotation is displayed on a mechanical counter which reads to 0.1°. This indicator system for measuring the counter angle reproduces to ±0.1°, the limitation being in the reproducibility of Selsyn position.

B. Energy Spread in the Scattering Process

For most of the measurements a $\frac{1}{4}$-in. diameter hole has been used as the beam-defining slit. The energy spread in the beam, $\Delta E/E$, is therefore 1% or 1.6 Mev.

There will also be an energy spread across the target because of the energy loss of the beam in traversing the target. Four targets have been used in the experiments: Au¹⁹⁷, Ni (natural isotope mixture), Al²⁷, and CH₂ (polyethylene film) with thicknesses of 2.29, 2.23, 1.21, and 1.01 mg/cm², respectively (see Table I, Column 2). By assuming that the O¹⁶'s are completely stripped, the energy loss for the O¹⁶'s may be considered to be $4^2 = 16$ times that of alpha particles of the same velocity.[28] The energy losses so determined are given in Table I, Column 3. If the population of particles is evenly distributed across both the target and the beam energy spreads (rectangular energy distribution), then the combination of the two spreads will be a trapezoidal distribution with full width at half maximum equal to the larger energy spread. Column 5 in Table I gives this total energy spread determined from the values in Columns 3 and 4. The significance of this energy

spread for the scattering process will be seen in the next subsection.

C. Angular Resolution of the Scattering

A number of factors contribute to the spread in the scattering angle when scattered particles are being detected by the counter at a fixed angle. First of all, there is a smearing out of the diffraction pattern produced by the scattered particles because of the spread in scattering energy just discussed. A rough estimate of this effect can be made by the following classical argument. Suppose that the diffraction pattern is determined by some interaction radius R between the target and the bombarding particle. Then, for a bombarding energy E, R is related to the center-of-mass scattering angle ϕ by

$$R = (ZZ'e^2/2E)[1 + \csc(\phi/2)], \qquad (1)$$

if Rutherford scattering is assumed. For a different energy, $E + \Delta E$, and the same interaction radius, R, there will be a different scattering angle $\phi + \Delta\phi$ where

$$\Delta\phi = -2\tan(\phi/2)[1 + \sin(\phi/2)]\Delta E/E. \qquad (2)$$

Equation (2) will be used in the following to estimate the $\Delta\phi$ introduced by the ΔE.[29] Using the largest scattering angle in the experiments (center-of-mass value), for each target material, $\Delta\phi$ was calculated from Eq. (2) for the values given in Table I, Column 5. $\Delta\theta$, the spread in laboratory angle corresponding to the $\Delta\phi$ thus calculated, is given in Table II, Column 3, using the value of $\Delta\phi/\Delta\theta$ given in Column 2.

A second factor contributing to the angular resolution is the multiple scattering in the target. Using the calculations of Williams,[30] this effect was evaluated and is displayed in Column 4 of Table II. There is also multiple scattering by the windows of the scattering chamber and counter as well as by the air path between them. The magnitude of this effect is given in Column 5.

Finally, the angular spread is increased because of the range in angles detected at any one time by the counter. For a $\frac{1}{4}$-in. diameter beam striking the target and a $\frac{1}{4}$-in. diameter counter located 21 in. from the target, the range in angle detected (full width at half maximum) would be about 0.70° in the laboratory. This value is entered in Column 6 of Table II.

The angular resolution resulting from combining all of these effects is entered in Column 7 of Table II. This result is found by taking the square root of the sum of the squares of Columns 3, 4, 5, and 6 (this procedure assumes that four Gaussian distributions are folded together). Finally, the angular resolution in the center-of-mass system is obtained by multiplying the

[28] L. C. Northcliffe has taken unpublished data for O¹⁶'s and alpha particles in aluminum which bear out this relationship.

[29] E. Goldberg and H. L. Reynolds, reference 16 and private communication, have calculated the $\Delta\phi$ associated with a ΔE using the Blair sharp cutoff approximation for several cases. They find values for $\Delta\phi$ smaller than the values in Eq. (2) by a factor of 1.5 to 2. However, Eq. (2) will be used in the following rough estimates because of its simplicity.

[30] E. J. Williams, Phys. Rev. 58, 292 (1940).

TABLE II. Angular resolution of the scattering measurement.

1 Target element	2 $\Delta\phi/\Delta\theta$	3 $\Delta\theta$ due to ΔE (degrees)	4 $\Delta\theta$[a] target multiple scattering (degrees)	5 $\Delta\theta$[a] window multiple scattering (degrees)	6 $\Delta\theta$[a] due to beam and counter size (degrees)	7 $\Delta\theta$[a] total (degrees)	8 $\Delta\phi$[a] total (degrees)
Au¹⁹⁷	1.08	0.92	0.55	0.50	0.70	1.37	1.48
Ni	1.27	0.52	0.38	0.50	0.70	1.07	1.36
Al²⁷	1.59	0.24	0.20	0.50	0.70	0.90	1.44
CH₂	2.33	0.19	0.13	0.50	0.70	0.90	2.08

[a] Full width at half maximum.

$\Delta\theta$ in Column 7 by $\Delta\phi/\Delta\theta$ in Column 2. The results are tabulated in Column 8. The resolution is 1.5° for all targets except carbon where it is 2°. Except for the gold target the main contribution to the angular spread is the beam and counter geometrical size.

D. Accuracy of the Scattering Angle

As stated in subsection A, the angular setting of the counter is reproducible to 0.1°. The linearity of the angular scale is even better than this value since 0.1° corresponds to $\frac{1}{3}$ of a tooth on the 1400-tooth angle-indicating gear. There remains then the accuracy of the lineup of the zero degree angle with the beam axis. The lineup was done in two ways: one, by lining up optically the counter with the beam slit and the center of the target; two, by scattering at 8° on both the left and right side of the beam. These two methods agreed to within ±0.1° so that the angle of the scattering is known to this accuracy. However, nonreproducibility of data at small angles indicates that the beam axis may have varied several tenths of a degree during the course of any particular run.

E. Monitoring and Normalization of the Scattering Cross Section

As stated in subsection A, the Faraday cups have not yet been calibrated so that the magnitude of the beam striking the target is not known. Also, the Faraday cups were usually not used for monitoring because they did not catch all of the beam.

The target was used as the monitor for the Au¹⁹⁷ and Ni targets. It was found that at the small scattering angles, the differential scattering cross section for these elements followed within a few percent the Rutherford $csc^4(\phi/2)$ angular dependence. The cross sections for these two elements were therefore normalized to the Rutherford cross sections at these angles.

The scattering from the Al²⁷ target was monitored also with the signal from the target. A subsidiary experiment with a large Faraday cup showed that the efficiency of the targets in measuring the beam intensity is the same for both the Al²⁷ and the Au¹⁹⁷ targets. Using this information and the thicknesses of the Al²⁷ and the Au¹⁹⁷ targets, the Al²⁷ cross sections were normalized to the Au¹⁹⁷ cross sections.

The scattering from the CH₂ target was monitored

with the smallest Faraday cup ($\frac{1}{4}$ in. wide). The Faraday cup was necessary because the CH₂ film is an insulator. The small cup, which may not have intercepted all of the beam, had to be used in order to get into as small scattering angles as possible. In spite of this, the data were quite reproducible. Normalization of the relative cross sections has not yet been made for the CH₂ target. Because of the absence of checks on the method of normalization, the Al²⁷ absolute cross-section values are reliable to only about 30–40%. The Au¹⁹⁷ and Ni cross sections are reliable to about 15% since they are fitted to the Rutherford curve.

F. Uniqueness of Particle Detection

Elastically scattered O¹⁶'s are easily distinguished from most other particles that can be emitted by the target because of their high unique energy, and their short range. The CsI(Tl) scintillator thickness (0.010 in.) has been chosen to just stop the 158-Mev O¹⁶'s. The maximum energy loss in the scintillator for alpha particles and protons is 22.5 Mev and 5.6 Mev, respectively. The pulse-height ratios for these three particles then are 100:30:8.5, respectively, for the O¹⁶'s, the alpha particles, and the protons.[31] The O¹⁶'s are therefore easily distinguished from these other particles. Also, because of the high energy of the O¹⁶'s as compared to nuclear gamma-ray energies, and the poor efficiency of the thin scintillator for detecting gamma rays, the gamma-ray background is negligible.

There are, however, two types of interactions in the target that can be confused with the elastic scattering process. One is an inelastic scattering process where the target nucleus is excited. This will be considered in the next subsection. The other process is the nucleon transfer interaction where one or more nucleons are transferred from the O¹⁶ to the target nucleus or vice versa. Here the detected particle (O¹⁵, say) is very similar to O¹⁶ and in some cases has almost the same energy. It may be demonstrated however, that the cross section for this reaction can be neglected. Volkov, Pasiuk, and Flerov[32] and Hubbard and Merkel[33] have

[31] Quinton, Anderson, and Knox, Phys. Rev. 115, 886 (1959).
[32] Volkov, Pasiuk, and Flerov, J. Exptl. Theoret. Phys. U.S.S.R. 33, 595 (1958) [translation Soviet Phys. JETP 6, 459 (1958).
[33] E. L. Hubbard and G. Merkel, Proceedings of the Conference on Reactions between Complex Nuclei, Oak Ridge National Laboratory Report ORNL-2606, 1958 (unpublished).
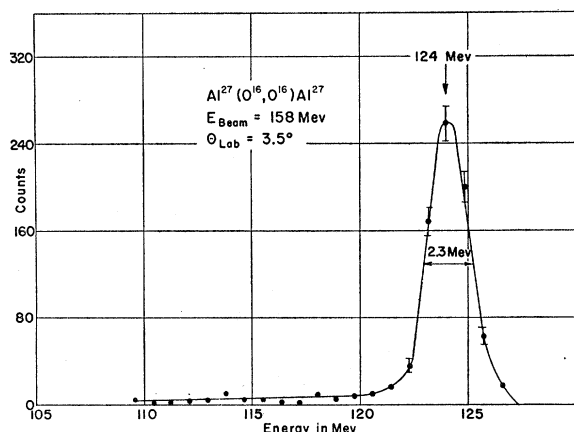
FIG. 2. Pulse-height distribution from the scintillation detector at 3.5° laboratory angle for O^{16} scattered by Al^{27}. Beam energy =158 Mev.

shown that most of the transfer reaction particles are emitted at an angle corresponding to an interaction distance of $\geqslant 1.4(A_1^{\frac{1}{3}}+A_2^{\frac{1}{3}})$ fermis (1 fermi$=10^{-13}$ cm), where A_1 and A_2 are the atomic numbers of the target and bombarding nuclei. Since the interaction distance for elastic scattering is comparable to this,[17] the scattering cross section will be near the Rutherford value at angles where transfer reaction products are emitted. The Rutherford scattering cross sections at these angles are of the order of 10^{-24} cm² while the nucleon transfer cross sections are of the order of 10^{-26} cm². The contribution of the transfer reaction to the elastic scattering cross section therefore may be neglected. In addition to this, the negative Q value of most nucleon transfer reactions is sufficiently large so that the reaction products have energies small enough to be distinguished from the elastically scattered particles.

G. Energy Resolution of the Scintillation Counter

The pulse-height distribution from the CsI(Tl) scintillator is analyzed with a 20-channel analyzer. The pulse-height values are then converted to energy values using data of Quinton, Anderson, and Knox.[31] The resulting energy spectrum for 158-Mev O^{16}'s scattered from Al^{27} at 3.5° in the lab system is shown in Fig. 2. Two points should be noted about this spectrum. First, the energy of the O^{16}'s in the peak is 124 Mev instead of the beam energy of 158 Mev because of energy loss in the target and in the windows before the O^{16}'s reach the scintillator. Second, the full width at half-maximum is 2.3 Mev. Since the spread in beam energy is $\sim 1\%$ or 1.6 Mev, the counter and windows add only 0.7 Mev or about $\frac{1}{2}\%$ to the resolution. The 2.3-Mev width in Fig. 2 determines the energy resolution of the counting system. Of the four targets studied, only the C^{12} nucleus has its first energy level at a sufficiently high energy so that elastically and inelastically scattered O^{16}'s can be distinguished.

Figure 3 shows that, indeed, the elastic scattering from the C^{12} can be distinguished from the inelastic scattering. The positions for the inelastic scattering resulting from exciting the lower levels in C^{12} and in O^{16} are shown by arrows above the spectrum. The inelastic peak is seen to be near the 4.4-Mev C^{12} level. The second inelastic experimental peak is near an excitation value of 12 Mev where there are many levels in both C^{12} and in O^{16}. It should be noted here that scattering by the hydrogen in the CH_2 target can be ignored; because of the kinematics, no O^{16} can scatter through an angle larger than 4° in the laboratory system.†

While elastic scattering clearly can be distinguished from the inelastic scattering for the C^{12} target this is not true for the Au^{197}, Ni, and Al^{27} targets because of their low-lying energy levels. For small-angle scattering, where the elastic scattering cross section is large, the elastic scattering will undoubtedly predominate over
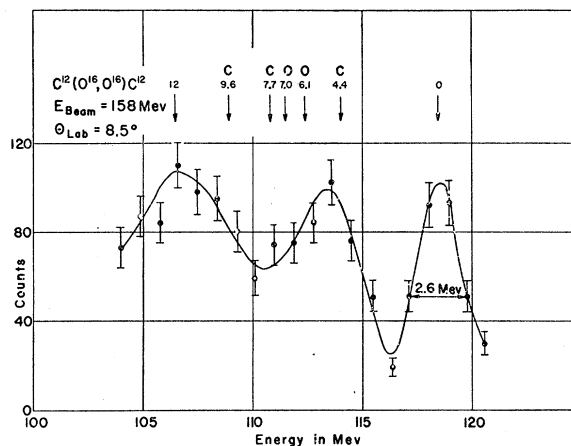

FIG. 3. Pulse-height distribution from the scintillation detector at 8.5° laboratory angle for O^{16} scattered by C^{12}. Beam energy =158 Mev. Arrows above the curve indicate the energy levels in C^{12} and O^{16}.

the inelastic scattering.[13,14] However, at the larger angles the elastic scattering cross sections decrease by a factor of 100 or more. Inelastic scattering then becomes significant as is shown in Fig. 4 for O^{16} scattered from Al^{27} at 12° in the lab. The peak has widened significantly compared to the peak in Fig. 2 and there is a low-energy tail on the peak presumably corresponding to inelastically scattered O^{16}'s. The energy levels for aluminum are also indicated in the figure and certainly inelastic scattering exciting the first two levels could be included in the elastic scattering peak. For this reason, the elastic scattering cross sections measured at the larger scattering angles represent an upper limit for the true cross sections.

† *Note added in proof.*—Anderson, Knox, Quinton, and Bach (submitted to Phys. Rev. Letters) have shown that the cross section for the production of stable nuclei such as N^{14} and C^{12} from targets bombarded by O^{16} is comparable to the elastic scattering cross section. The lowest energy peaks in Figs. 3 and 4 may therefore be produced by these nuclei.

H. Correction to the Scattering Cross Section Due to Angular Resolution

Chase and Cox[34] have analyzed the effect of the counter detecting scattered particles over a range of angles. For small angles, and assuming a circular aperture at the counter and a Rutherford scattering cross section, there is an error introduced into the measured cross section, σ_{meas}, of

$$(\sigma_{meas} - \sigma_{true})/\sigma_{true} = (\Delta\phi/\phi)^2, \qquad (3)$$

ϕ being the scattering angle in the center-of-mass system. Here σ_{true} is the true cross section and $\Delta\phi$ is given in Column 8 of Table II. For $\Delta\phi \sim 1.5°$, and $\phi = 5°$, the error introduced by this process is $\sim 10\%$. At larger angles, the effect rapidly becomes negligible.

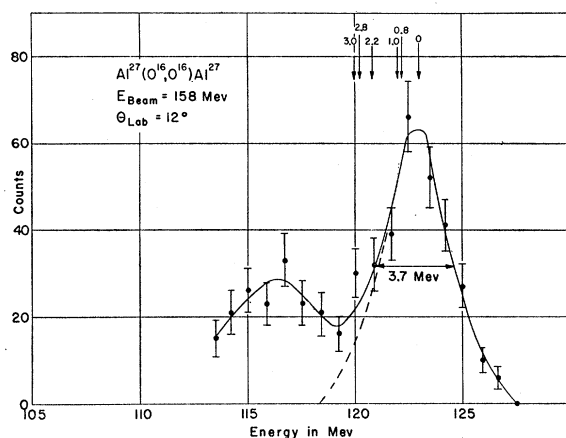FIG. 4. Pulse-height distribution from the scintillation detector at 12° laboratory angle for O¹⁶ scattered by Al²⁷. Beam energy = 158 Mev. Arrows above the curve indicate the energy levels in Al²⁷.

III. RESULTS AND DISCUSSION

A. Au¹⁹⁷

The elastic scattering differential cross sections in the center-of-mass system, $\sigma(\phi)$, for O¹⁶ on Au¹⁹⁷ are shown in Fig. 5. The ordinate plotted is σ/σ_R where σ_R is the Rutherford scattering differential cross section. The abscissa is ϕ, the center-of-mass scattering angle. The O¹⁶ beam energy in the center-of-mass system is 145 Mev. The angular resolution of the experiment is indicated above the data in Fig. 5. The cross section σ is seen to follow with small fluctuations the Rutherford value out to an angle of about 25°. At this point σ rises above σ_R until at 30° it is about 30% above σ_R. At larger angles it drops rapidly below σ_R. This general structure for $\sigma(\phi)$ is typical of elastic scattering by heavy elements for both alpha particle[4-8] and C¹² beams.[17] The smaller fluctuations about this general structure shown in Fig. 5 appear to be real but they have not yet been repeated experimentally. As mentioned in Sec. II G, inelastic scattering cannot be

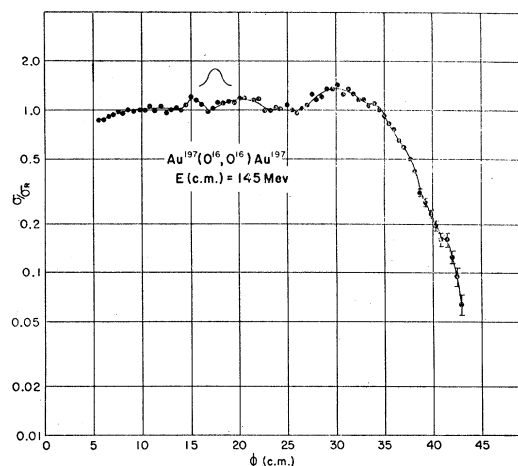[34] C. T. Chase and R. T. Cox, Phys. Rev. 58, 243 (1940).

FIG. 5. Angular distribution in the center-of-mass system of O¹⁶ elastically scattered by Au¹⁹⁷. The center-of-mass energy is 145 Mev. σ is the experimental differential scattering cross section in the center-of-mass system. The Rutherford differential scattering cross section is $\sigma_R = 2.47 \times 10^{-26} \csc^4(\phi/2)$ cm²/sterad.

distinguished from the elastic scattering for Au¹⁹⁷. Experimentally, the effect of inelastic scattering becomes noticeable when the elastic scattering peak becomes broadened (see Figs. 2 and 4). Such broadening is not found to occur at the angles shown in Fig. 5. A broadening here, of course, is only a sufficient but not a necessary condition for proof of inelastic scattering.

B. Ni (Natural Isotopic Abundance)

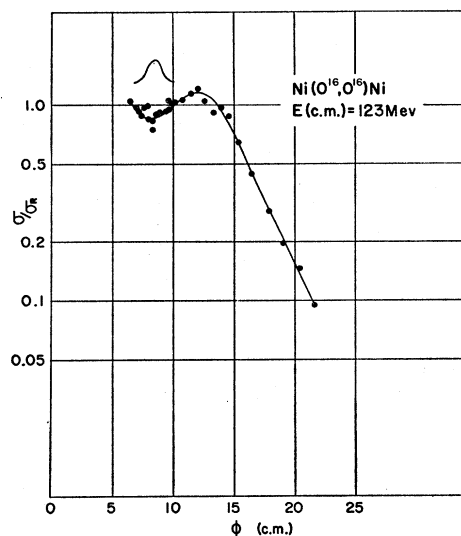Figure 6 shows the results of scattering of O¹⁶ by Ni. The similarity to the general form of the Au¹⁹⁷ data

FIG. 6. Angular distribution in the center-of-mass system of O¹⁶ elastically scattered by Ni (normal isotopic abundance). The center-of-mass energy is 123 Mev. σ is the experimental differential scattering cross section in the center-of-mass system. The Rutherford differential scattering cross section is $\sigma_R = 4.30 \times 10^{-27} \csc^4(\phi/2)$ cm²/sterad.
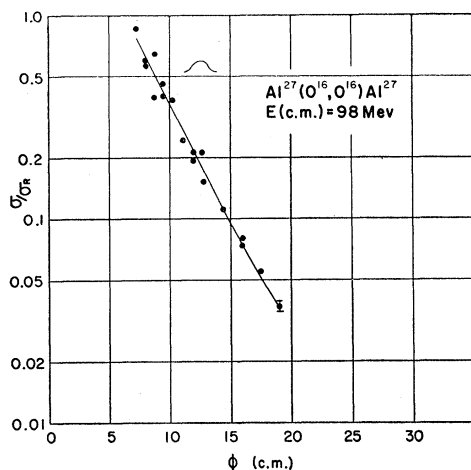
FIG. 7. Angular distribution in the center-of-mass system of O^{16} elastically scattered by Al^{27}. The center-of-mass energy is 98 Mev. σ is the differential scattering cross section in the center-of-mass system. The Rutherford differential scattering cross section is $\sigma_R = 1.45 \times 10^{-27} \csc^4(\phi/2)$ cm^2/sterad.

in Fig. 5 is clear, i.e., Rutherford scattering at the smallest angles is followed by a rise above Rutherford scattering and then a steep drop below the Rutherford value. The outstanding difference between these two curves is that the drop away or break from the Rutherford scattering value occurs at a smaller scattering angle. The reason for this change in the break angle has been explained by Blair[3] in terms of partial waves centered around the classical trajectory of the scattered particle. Classically, a smaller Z for the target nucleus will give a smaller scattering angle for the same apsidal distance for the particle trajectory. Therefore, the nickel nucleus interrupts particle trajectories at smaller scattering angles than does the gold nucleus (ignoring the change in the nuclear radius which is small) and the scattering drops below Rutherford scattering at smaller angles. Inspection of the scattering pulse-height distributions indicates that inelastic scattering becomes significant at angles greater than 18°. Thus, the cross sections plotted in Fig. 6 at angles larger than this are upper-limit values.

It is instructive to compare the Ni(O^{16},O^{16})Ni scattering to the scattering of alpha particles by a nucleus with a similar Z, namely copper. Comparison will be made at a "classically corresponding" energy, i.e., at an energy where $ZZ'e^2/2E$ is the same for both the O^{16} and the alpha-particle scattering. The Rutherford cross sections $[\sigma_R = (ZZ'e^2/4E)^2 \csc^4(\phi/2)]$ and the apsidal distances $\{R = (ZZ'e^2/2E)[1 + \csc(\phi/2)]\}$ will then be the same for a given scattering angle.[35]

---

[35] When recoil is significant in the scattering problem exact "classically" corresponding conditions cannot be obtained because of the following. In Newton's second law of dynamics, $F = ma$, where F is the force on the bombarding particle and m is its mass; classical correspondence then occurs when F is proportional to m such as in a gravitational problem. In scattering without recoil, this feature also prevails since $F = ZZ'e^2/r^2$ and $Z' \propto m$. However,

Neglecting recoil, the classically corresponding energy to 160-Mev O^{16}'s is 40-Mev alpha particles. Inspection of Cu(α,α)Cu scattering results[12] at 40 Mev shows a definite diffraction pattern superimposed on the scattering cross-section curve in the region of falling away from Rutherford scattering in contrast to the smooth drop off in the Ni(O^{16},O^{16})Ni pattern. The quantum-mechanical diffraction effects are thus different for these classically corresponding situations. Indeed, Blair[36] has predicted that the scattering of particles heavier than alpha particles would result in decreased diffraction effects for classically corresponding conditions due to the increase in η. The classical similarities are still apparent however, in that the Cu(α,α)Cu curve drops away from the Rutherford scattering in approximately the same angular region as the Ni(O^{16},O^{16})Ni curve.[37]

C. Al^{27}

The results of $Al^{27}(O^{16},O^{16})Al^{27}$ scattering are shown in Fig. 7. Again, the sharp drop away from the Rutherford cross section is observed and the breakaway is at still smaller angles than with either Au^{197} or Ni. In
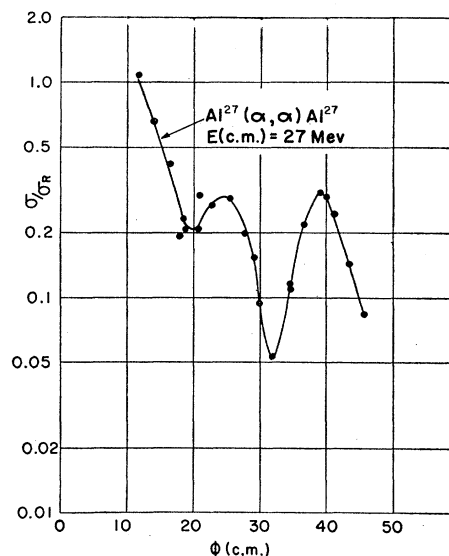

FIG. 8. Angular distribution in the center-of-mass system of alpha particles elastically scattered by Al^{27}. The center-of-mass energy is 26 Mev. σ is the experimental differential scattering cross section in the center-of-mass system. The Rutherford differential scattering cross section is $\sigma_R = 1.28 \times 10^{-27} \csc^4(\phi/2)$ cm^2/sterad.

---

with recoil, $F = \mu a$ in Newton's law where μ is the reduced mass. The electrostatic force is still $F \propto Zme^2/r^2$ and so classical correspondence can no longer occur.

[36] J. S. Blair (private communication).

[37] J. S. Blair, reference 3, has pointed out that the "classical" angle corresponding to the trajectory that grazes the nucleus is that angle for which $\sigma/\sigma_R \sim \frac{1}{4}$. For Ni($O^{16}$,$O^{16}$)Ni, $\phi_{1/4} = 18.5°$; while for Cu(α,α)Cu, $\phi_{1/4} \sim 20°$. The Ni(O^{16},O^{16})Ni angle would be expected to be somewhat smaller since the interaction radius is the sum of the radii of the target and bombarding nuclei and the O^{16} nucleus is larger than the alpha particle.

fact, the angles for Rutherford scattering are too small to be detected at the present. Inelastic scattering very likely contributes to the cross sections plotted at angles greater than 15°.

Comparison of Fig. 7 to alpha-particle scattering reveals an even greater change in scattering curve structure than was true for the Ni case. Al(α,α)Al scattering at 40 Mev shows[12] only diffraction structure although there may be a drop below Rutherford scattering at angles smaller than those measured. However, because of recoil, the center-of-mass energy for the O^{16} scattering is only 98 Mev so that the "classically corresponding" energy for alpha particles is 25 Mev in the center-of-mass system (deeping $ZZ'e^2/2E$ fixed). Thus a comparison with 40-Mev scattering is not too reliable. However, Al(α,α)Al data have also been taken at 19 Mev[14] and these data also show only a diffraction pattern with no drop away from the Rutherford value. Nevertheless, in order to make a more direct check, an Al(α,α)Al experiment was performed at 26 Mev which is close to the classically corresponding energy of 25 Mev. The results of this experiment are shown in Fig. 8. Normalization of the data was made by measuring $Au^{197}(\alpha,\alpha)Au^{197}$ cross sections at small angles and normalizing these to the Rutherford cross section. It is seen that strong diffraction effects are present,[38] in sharp contrast to the steep drop off shown in Fig. 7 for Al(O^{16},O^{16})Al scattering. There is also, however, a drop below Rutherford scattering at the small angles along with the diffraction structure. In fact, the curve as a whole is remarkably similar to curves calculated by Blair using the sharp cutoff model,[15] i.e., the drop away from Rutherford scattering extends over something like a decade and then strong
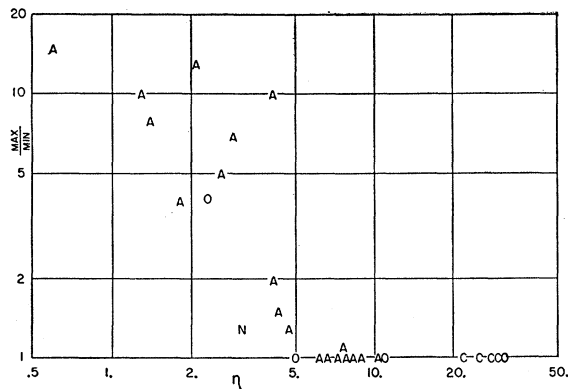

FIG. 9. The ordinate is the ratio of the maximum to minimum for angular distribution diffraction patterns. The abscissa is $\eta = ZZ'e^2/\hbar v$. The data are taken from various scattering experiments reported in the literature. See Table III for the data and references. The letters indicate the bombarding particle: A = alpha particle, C = C^{12}, N = N^{14}, O = O^{16}.

[38] It should be noted that the energy resolution again was not sufficiently good to eliminate possible inelastic scattering so that, particularly at the diffraction minima, there may be significant inelastic contributions to the cross sections plotted.

TABLE III. Summary of elastic scattering measurements.

η	Z'	Z	E_{lab}	(Max/min)	Reference
0.6	2	6	40	15	a
1.3	2	13	40	10	a
1.5	2	10	18	8	b
1.9	2	13	19	4	c
2.2	2	22	40	13	a
2.4	8	6	158	4	d
2.7	2	18	18	5	b
2.9	2	29	40	7	a
3.2	7	4	27	1.3	e
4.1	2	41	40	10	a
4.2	2	29	19	2	c
4.3	2	47	48	1.5	f
4.7	2	47	40	1.3	a
5.3	8	13	158	1	d
6.3	2	47	22	1	g
6.8	2	47	19	1	c
7.2	2	79	48	1	f
7.3	2	73	40	1	h
7.5	2	82	48	1.1	f
7.9	2	79	40	1	h
8.3	2	82	40	1	h
9.0	2	90	40	1	h
10.6	2	79	22	1	g
11.0	2	82	22	1	g
11.3	8	28	158	1	d
24	6	79	118	1	i
26	6	79	101	1	i
29	6	79	79	1	i
30	6	79	74	1	i
32	8	79	158	1	d

a See reference 12.
b See reference 13.
c See reference 14.
d This paper.
e M. L. Halbert and A. Zucker, Phys. Rev. 115, 1635 (1959).
f See reference 7.
g See reference 4.
h See reference 5.
i See reference 17.

diffraction sets in. Unfortunately, the experimental normalization is somewhat uncertain.

D. General Remarks

From the data presented, certain features of the scattering angular distribution curves become evident. One is, that for a higher Z' for the bombarding particle, less diffraction occurs (as Blair has predicted[36]). Also, Igo, Wegner, and Eisberg[12] have pointed out that for higher Z for the target nucleus and for lower bombarding velocity less diffraction occurs. Since the strength parameter for the Coulomb interaction, $\eta \equiv ZZ'e^2/\hbar v$, contains all of these variables it is interesting to investigate the occurrence of diffraction as a function of η.

It is clear from the previous remarks that as η decreases the diffraction structure will increase. To make this statement more precise, the plot in Fig. 9 has been constructed. The data for the plot are given in Table III. In Fig. 9 the abscissa is the $\eta = ZZ'e^2/\hbar v$ for the angular distribution in question, the ordinate is the ratio of the maximum to the minimum for the diffraction features of the angular distributions. The ratio is designated as unity for the cases of no diffraction. Reference to the angular distributions from whence these data originate will reveal that the maximum/
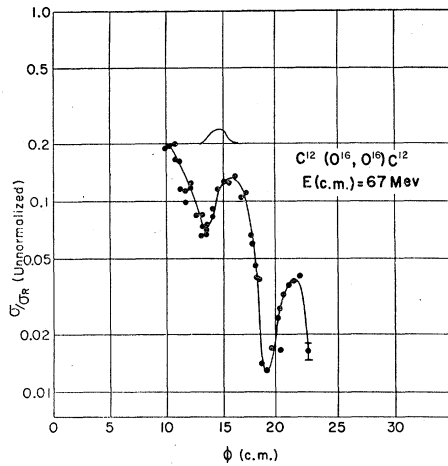
FIG. 10. Angular distribution in the center-of-mass system of O^{16} elastically scattered by C^{12}. The center-of-mass energy is 67 Mev. σ is the experimental differential scattering cross section in the center-of-mass system. The Rutherford differential scattering cross section is $\sigma_R = 6.66 \times 10^{-28}$ cm^2/sterad.

minimum ratio is only a qualitative value since the amplitudes of the several diffraction peaks in an angular distribution often vary a factor of two or more. Nevertheless, Fig. 9 demonstrates the conclusion that the diffraction effects depend strongly on the value of η in the scattering process. For η greater than 5 there is very little diffraction while for η decreasing below 5, diffraction rapidly sets in. A represents alpha-particle scattering; C, carbon scattering; N, nitrogen scattering; and O, oxygen scattering.

E. C^{12}

An experimental test of the importance of η in determining diffraction structure has been performed by scattering O^{16} from C^{12} at 158 Mev in the laboratory system (67 Mev in the center-of-mass system). η, for this situation, is 2.3 so that diffraction would be expected. The result of the experiment is shown in Fig. 10 and diffraction is clearly evident. This result has been included in Fig. 9 and in Table III. It is seen to fit well with the trend of the rest of the data. It should be noted that the curve in Fig. 10 is unnormalized. Since the inelastic scattering is distinguished for the carbon scattering the diffraction pattern represents only elastic scattering. The angular resolution, as indicated in Fig. 10, however, may be sufficiently wide to fill in to some extent the diffraction structure. Also,
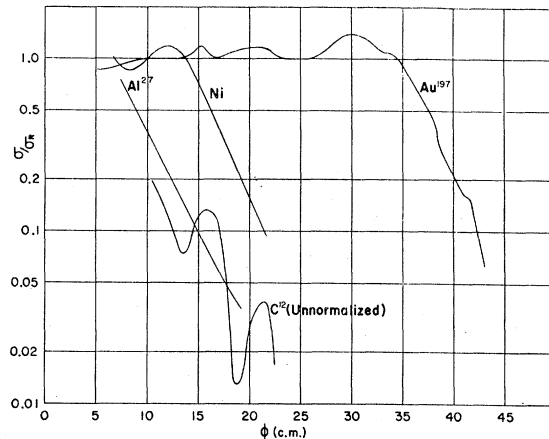

FIG. 11. A composite drawing of the curves of Figs. 5, 6, 7, and 10.

the two diffraction peaks in Fig. 10 were taken on different days so that their relative magnitudes may be somewhat in error.

The curves of Figs. 5, 6, 7, and 10 are plotted together in Fig. 11 for comparison.

F. Nuclear Radii

The qualitative nature of the data presented does not permit accurate nuclear radii determinations. However, by using the angle where $\sigma/\sigma_R = \frac{1}{4}$ as the angle corresponding to the classical trajectory that is tangent to the nucleus,[3] an interaction radius can be determined for each of the scattering experiments. The radii so determined for Au^{197}, Ni, and Al^{27} are all consistent with a radius of $1.5(A_1^{\frac{1}{3}} + A_2^{\frac{1}{3}})$, where A_1 and A_2 are the nuclear weights of the interacting nuclei. The spacing of the diffraction structure in the C^{12} data also agrees with such a radius expression.

ACKNOWLEDGMENTS